Ultrasonic welding of CF/PEEK composites: Influence of welding parameters on interfacial temperature profiles and mechanical properties

Margot Bonmatin, France Chabert, Gérard Bernhart, Thierry Cutard, Toufik Djilali

Ultrasonic welding of CF/PEEK composites: Influence of welding parameters on interfacial temperature profiles and mechanical properties

Margot Bonmatin [a,b], France Chabert [a,*], Gérard Bernhart [b], Thierry Cutard [b], Toufik Djilali [c]

[a] INP-ENIT, University of Toulouse, 47 Avenue d'Azereix, 65016 Tarbes, France
[b] Institut Clement Ader (ICA), University of Toulouse, CNRS, IMT Mines Albi, INSA, ISAE-SUPAERO, UPS, Campus Jarlard, 81013 Albi, France
[c] Lauak Innovative Solutions, Lauak Group, Parc d'activité Cognac, 8 Rue Louis Caddau, 65000 Tarbes, France

A B S T R A C T

This work focuses on ultrasonic (US) welding of CF/PEEK composite containing a PEI layer at the interface. Welding time, load and amplitude are defined as the welding parameters. The influence of each parameter is assessed by temperature measurement and mechanical tests on US welding specimens. 80-μm diameter thermocouples are integrated into the interfacial polymer layer for in-situ monitoring of the maximum temperature profile during the welding phase. Only welding time and welding load have an influence on both temperatures and lap shear strengths (LSS). The highest LSS are close to 50 MPa, and the temperature achieved in those cases is around 580°C. Interfacial fractures occur in both PEI and PEEK. PEI-based fracture is mostly brittle whereas PEEK-based fracture is a competition between brittle and ductile fracture. Finally, a fracture within the PEI/PEEK blend can occur. Raman spectroscopy is effectively used to quantify the thickness of this blend zone, it is about 0.075 mm.

1. Introduction

The growing use of thermoplastic (TP) composites in the industry comes with its challenges and limitations. They are known to decrease structural weight and processing costs. Despite those advantages, the assembly of several parts has to be worthwhile. Otherwise, TP composites cannot claim a significant and sustainable use in the industrial sector. Nevertheless, a significant issue arises from the joining of two composite parts. Mechanical fastening, adhesive bonding and welding are the three main viable approaches available in the industry. However, fiber fracture and heavier composite structures are inevitable outcomes using mechanical fastening. Surface preparation might be needed considering adhesive bonding which can turn out to be time consuming. In order to overcome the disadvantages, welding is considered to be a reasonable answer to this issue [1].

Several processes exist to weld thermoplastic composites that can be separated into three classes of processes according to Yousefpour et al. [1]: thermal welding, electromagnetic welding and friction welding. The difference between the three depends on how heat is generated at the interface. Thermal welding requires an external heat source for the parts to be welded. A high frequency electromagnetic field is used to heat the interface in electromagnetic welding processes. In the third case, the motion between the two parts induces a friction phenomenon which causes the temperature to rise at the interface. In the aerospace industry, welding is considered to be a promising way of assembling parts since it decreases the weight of structural parts while increasing manufacturing rates. There are currently two processes industrially used and, namely resistance and induction welding. However, they both display relatively high welding time (above a few minutes) and require high energy level, especially induction welding [2].

Polymer welding has been studied for years to join thermoplastics parts with a precise and strong adhesion [3]. Voyutskii [4] and Vasenin [5] state the autohesion mechanisms based on the diffusion of macromolecules in 1960s. Then, De Gennes [6,7] and Brochard-Wyart [8] exposed the theory of reptation which describes the motion of chains above the glass transition for amorphous thermoplastics. This theory was successful in predicting the molecular weight dependency of the self-diffusion across the interface of two identical polymeric surface. Then, the process parameters (temperature, pressure, time) were related to the interfacial strength of welds. The most famous equation is Wool's model [9], predicting the energy required to separate the joined parts as a function of time, pressure, temperature and molecular weight. Interdiffusion of macromolecules occurs when two polymer surfaces are brought into close contact, the interdiffusion becomes more likely when the temperature is higher than the polymer glass transition temperature and the interdiffusion accelerates as temperature increases. Besides temperature, another crucial parameter is the contact area between

* Corresponding author.
E-mail address: fchabert@enit.fr (F. Chabert).

the two surfaces of the assembly. This area depends on the roughness of each substrate. It evolves to intimate contact as soon as the polymer flows because the surface asperities get squeezed. The interfacial strength is at maximum when reaching the intimate contact. Several models have been proposed to predict the evolution of this contact with temperature, time and pressure while considering the rheological behavior of the polymer and roughness parameters [10–13]. The degree of intimate contact is defined as the contact area ratio, it is 1 when the perfect contact is reached. In this study, we used PEI as the energy director. PEI will easily flow into the interfacial zone due to its low viscosity compared to those of PAEK. Consequently, it is expected that PEI fills the asperities of the PAEK composites to be welded. For this reason, we assume the degree of intimate contact is close to 1.

To obtain a good weld, a compromise between time, pressure and temperature is necessary. The challenge is to succeed in heating the interface only. Otherwise, heating the entire thickness of the TP composite parts may cause deconsolidation of the composite layers as well as degradation of the polymer matrix. When welding thermoplastic composites or any thermoplastic based materials, the physical phenomena are the following: the material is heated until the macromolecules reach sufficient mobility to diffuse across the interface [3]. The required temperature to achieve this is above the glass transition temperature. At T_g or above, the polymer benefits from a certain degree of macromolecular mobility. Moreover, the higher the temperature, the faster the diffusion is. The diffusion times follow the arrhenius equation. For instance, Bonmatin et al. [14] have measured the diffusion times of PAEK. Also, an intimate contact created by applying a pressure between the two parts is mandatory to enhance the diffusion of chains. The latter can therefore entangle and create a bond.

Ultrasonic welding (USW) allows really fast cycle times (lower than 1 s) and it does not require the use of an external non-polymer-based material such as a susceptor. In the literature, studies on high performance thermoplastic composites, such as carbon fiber (CF)/poly(ether imide) (PEI) [15,16], CF/(poly(phenylene sulfide) (PPS) [17–19] or CF/poly(ether ether ketone) (PEEK) [20] can be found. During the process, the upper specimen to be welded vibrates vertically while the lower one is static. The friction phenomenon between the two specimens induces an increase of the interfacial temperature.

Ultrasonic (US) welding of pure polymers requires the use of a polymer-based material placed at the welding interface, called an energy director (ED). The energy director has usually a triangular shape to allow the energy to be directed at the interface. This technology is widely used in automotive industry and packaging. Composite US welding is derived from polymer US welding. Considering welding of thermoplastic composites to thermoplastic composites, the ED is usually the same as the polymer matrix for miscibility reason. The study on welding of dissimilar polymers are scarce. The stiffness of the polymer layer being lower than the composite, it concentrates the friction phenomenon at the interface, where heat is preferentially generated. US welding without ED is more likely to thermally affect the entire thickness of the specimens and it also reduces the joint mechanical strength [20]. In the first studies conducted by Benatar et al. [21], Liu et al. [22] & Villegas et al. [23,24], the energy directors had a triangular shape allowing the heat generation at the highest of the top of the ED. Nonetheless, the manufacturing of such materials is inconvenient since it requires the extrusion of a triangular shape in a mold. Villegas et al. [18] showed later that the use of a polymer film at the interface is easier and the mechanical strength of the welds are similar.

Specimens are usually welded into a single lap shear configuration which generates a closed contact between the specimens and hinders the use of temperature control or infrared thermography. Since usual monitoring techniques cannot be used for ultrasonic welding, studies were carried out on high performance thermoplastic composites to correlate the physical changes occurring during welding to the output data of the welding equipment [15,21] in order to monitor the process. It has been demonstrated that welding can be monitored by using power curves and the displacement of the sonotrode, both data from the welding equipment. The combination of these two parameters can be linked to the material physical structure evolution throughout welding. The sonotrode is a metal part of the device that vibrates vertically and comes into contact with the upper specimen. It also maintains the pressure instruction during welding. In some studies, this procedure led to the determination of optimum welding parameters and a stronger understanding of the influence of welding parameters [15–17,24,25]. The main flaw of ultrasonic welding is that optimum parameters only apply to one material and its specific configuration, i.e. thickness or geometry of the energy director for example. Until now, the parameters defined for one configuration do not suit another one, because of the lack of knowledge on the role of each welding parameter.

Temperature measurements during US welding is a major challenge since it could be an effective way of process monitoring and optimization. Knowing the temperature would give information about the physical structure of the polymer along welding. Therefore, welding parameters could be chosen in order to target the suitable temperature. Indeed, if you combined the rheological parameters of the polymer to the temperature measurement, it would possible to identify a range of parameters in which the specimens would diffuse and create an extremely good bond at the interface. Tao et al. used 0.125-mm-diameter thermocouples to assess temperature data during welding of CF/PEEK specimens [20] with and without PEEK ED. Thermocouples were placed between the two specimens prior welding. It appears that the use of an ED decreases maximal reached temperature (416 °C with ED versus 443 °C without ED), probably because heat is absorbed by the melting ED. It also increases the heating rate, which is due to viscoelastic heating of the polymer, as explained by the authors. To the best of our knowledge, this is the only study on experimental temperature profile measurements during USW of thermoplastic composites. Modeling thermal diffusion is an option to overcome the absence of experimental data.

Levy et al. [26] completed a finite element model on ultrasonic welding of CF/poly(ether imide) (PEI) using a flat PEI ED. They demonstrated that the heat is firstly generated at the edge of the contact area between the two specimens and that friction phenomenon is predominant at first but replaced by viscoelastic dissipation when temperature increases. Nonetheless, this shows that the interface temperature cannot be controlled and is hard to quantify.

To this end, this study focuses on USW of CF/PEEK specimens using PEI energy director. Since PEI is an amorphous polymer with a glass transition temperature of 220 °C, the aim is to weld without melting the PEEK matrix whose melting temperature is 340 °C. Such configuration is proposed as a way to prevent composite delamination and degradation during welding. Temperature evolution measurements were investigated coupled with output data from the welding equipment to evaluate physical changes of the material. Single lap shear strength and fracture surfaces were investigated to assess the influence of different welding parameter set. The objective is to link both temperature during welding and mechanical strengths in order to get a better understanding and control of the process. Then, the composition of the welded interfacial zone is analyzed through Raman spectroscopy to quantify the thickness of the PEI/PEEK blend.

2. Experimental procedure

2.1. Materials and sample manufacturing

APC-2 (CF/PEEK) ply composites were purchased from Cytec Industries. APC-2 consists of unidirectional carbon fibers into PEEK matrix. Out of autoclave consolidation process was used to manufacture 2 mm plates. Temperature cycle is presented in Fig. 1. It is supposed that this cycle do not alter the physical–chemical properties of the material integrity. Vacuum applied through a vacuum bag is - 50 mbar.

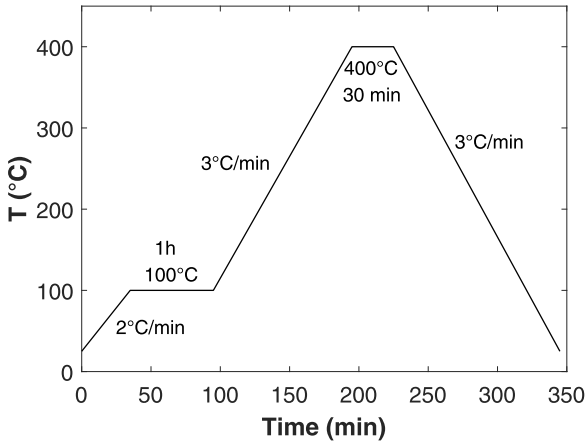

Fig. 1. Temperature cycle for manufacturing of welding specimens.

The 16 layers symmetrical cross-ply $[0,90]_{4S}$ sheets include an initial 0,25 mm-thick layer of PEI on one side for welding purposes. PEI film was purchased from Goodfellow as 610 x 610 mm^2 sheets. Welding specimens were then water jet cut in order to get rectangular shape of 25 x 100 mm^2 as recommended by NF EN 2243-1 standard. Prepreg and PEI film were dried at 105 °C for 4 h before stacking.

2.2. Welding equipment

Electrical Motion 20 ultrasonic welder from Rinco Ultrasonics was used for the experiments. It is an industrial equipment with a working frequency of 20 kHz and a maximum load of 3000 N. Welder can be divided in several components, as seen in Fig. 3:

- **A generator** that creates an ultrasonic wave,
- **A converter** that changes the electrical wave into a low amplitude vertical mechanical vibration,
- **A booster** that amplifies the vibration amplitude,
- **A sonotrode** that amplifies amplitude a second time, comes into contact with the upper specimen and applies the welding pressure.

Amplification provided by booster and titanium sonotrode are respectively 2 and 4. A clamping tool was designed in order to provide a vertical movement without parasite bending in order to ensure pure friction during welding test. The clamping tool is presented in Fig. 2.

Three welding parameters are considered in this study: the welding load (N), the peak-to-peak vibration amplitude (μm) and welding time (ms). The welding time is associated with the time during which the ultrasound are operating. The welding load continues to be applied during the selected 2500 ms cooling phase. The specimens are welded in a single lap configuration. Three layers of PEI film are used during welding, as it can be seen in Fig. 4: one PEI layer is included in each composite specimens, another one is placed between the two specimens.

2.3. Welding temperature measurements

Surface roughness is an important factor as heat will nucleate most likely at the contact areas during welding, that is why thermocouples need to be integrated into the polymer layer. 80-μm-diameter K-type thermocouples were integrated in the PEI layer prior welding in order to measure temperature evolution during welding and also avoid a protrusion at the welding interface. Chromel and alumel wires were manually arc welded to create the thermocouple. The thickness of the arc welded thermocouple was 80 μm. A dedicated integration procedure was defined taking advantage of PEI amorphous state that undergoes

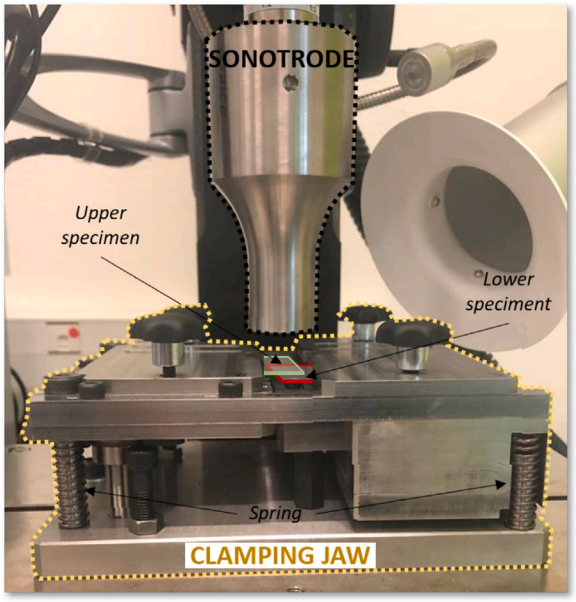

Fig. 2. Clamping tool for welding specimens.

a viscosity drop from Tg (220 °C) and allows the integration without melting of PEEK. A 25 N metallic weight was applied on top of the thermocouple and specimen in an autoclave heated at 290 °C for 40 min. A polyimide film was placed between the weight and PEI layer to ensure a repeatable roughness. Micrograph in Fig. 5 shows the embedded thermocouple within the polymer energy director.

2.4. Single lap shear tests

Single lap shear tests were conducted on an INSTRON 5800R tensile test equipment following the NF EN 2243-1 standard. Parallel shifted clamping jaws were used to avoid samples bending as much as possible. The experiments were conducted at 2800 N min^{-1}. The single lap shear strength (LSS) is deducted from the following equation:

$$LSS\ (\text{MPa}) = \frac{Maximum\ load\ (\text{N})}{Contact\ area\ (\text{mm}^2)}$$

2.5. Raman Spectroscopy

Raman map were made at the interface after welding, using a Horiba Yvon Jobin Labram HR 800 RAMAN confocal microscope. Raman sample is made from out-of-plane cutting of the weld. The sample was exposed to continuous laser radiation provided by a He/Neon laser at 633 nm, with a power of 8 mW. Attenuation filters have been used to avoid any degradation of the material, reducing the laser power by two. The map was produced using a motorized XYZ table with an accuracy of 0.1 μm and a measurement step of 1 μm. The spectrum of the map was acquired with a time of 10 s and 2 accumulations.

3. Results and discussion

3.1. Typical welding data

During ultrasonic welding, output data are registered by the welder control system all along each welding experiment, such as welding load, electrical power and sonotrode displacement. Welding load is a test set up parameter but its measurement allows a control of this value during welding. As seen in Benatar's and Villegas's works [17,21], power and travel (*i.e.* displacement of the sonotrode) data are used to

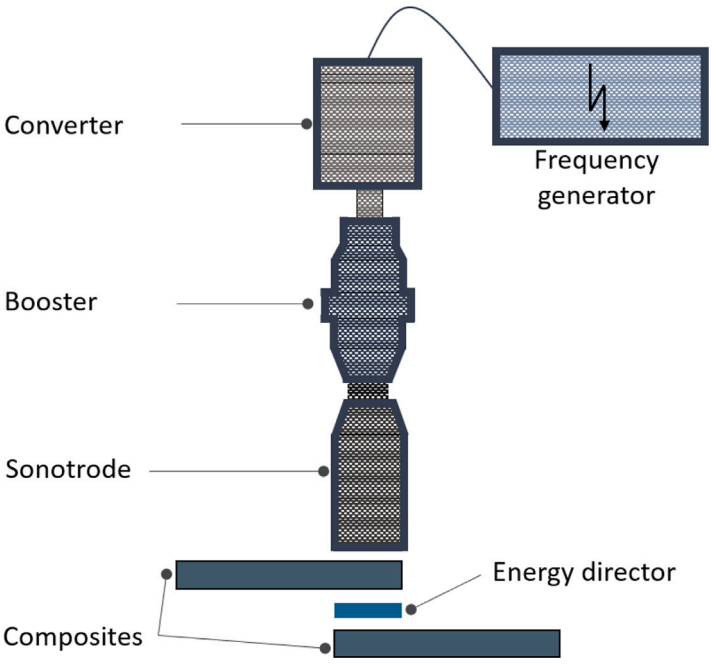

Fig. 3. Layout of the ultrasonic welding device.

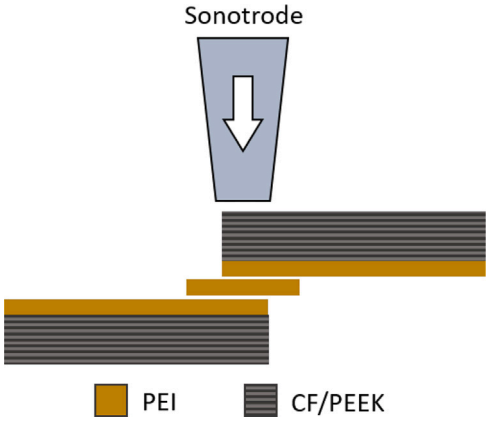

Fig. 4. PEI and CF/PEEK specimens configuration for welding.

understand the physical structure evolution of the material during the experiment and four stages can be defined.

While maintaining a constant load of 500 N during the duration of the ultrasonic impulsion, it can be seen in Fig. 6 that the sonotrode moves slightly upward during stage 1 until reaching a maximum after 300 ms. This can be associated with the heating mechanism of thermoplastics, that prone to expand when reaching melting or softening in the case of amorphous TP. It can also be noticed that the power curve exhibits a step rise during this heating phase of the polymer until reaching a peak at the same time as travel direction changes. According to Villegas [17], the decrease of both travel and power curves in stage 2 is associated with the local melting of the energy director and in our case, with the beginning of local softening of the PEI.

A second power rise is noticed in stage 3, which is related to the squeeze flow of PEI. Right after this second peak, the welding load curve shows that it is difficult to maintain its value at 500 N. We assume that high squeeze flow happens at the interface, forcing the sonotrode to go down to keep the 500 N welding load value. After reaching this second peak, the power curve reaches a plateau in stage 4, indicating that squeeze flow of PEI occurs and that PEEK starts melting. Villegas et al. [17] explained this plateau by a competition between the squeeze flow of the energy director and the local melting of the resin.

3.2. *Typical temperature curve*

Fig. 7 illustrates a typical temperature–time curve during welding. The graph displays temperature and sonotrode displacement (or travel) as a function of time. The displacement of the sonotrode is differential, *i.e.* it is the difference between the initial position of the sonotrode and its position all along the welding experiment. The temperature results are combined with the travel data registered from the welding equipment in order to better understand the physical phenomena occurring during welding. Indeed, the sonotrode goes up or down to maintain a constant load during welding. Its value gives an indication of the polymer swelling or flowing.

Looking at the curves in Fig. 7, the first observation is that the phenomena are fast since the time range is only 2 s. The characteristic time of the thermocouples used in this study are below 5 ms [27], meaning that those thermocouples are not a limitation for US welding. Several stages and breaking points are observed in Fig. 7. First of all, a very fast heating ramp at around 1000 K s^{-1} takes place in stage 1, during which a slight travel increase is seen. This means the polymer is swelling when heating due to thermal expansion, and the sonotrode goes up to maintain a constant welding load. A clear slope break is then observed at point 2 associated with the starting of decrease in travel. This point is associated with the beginning of PEI flow that continues until a maximal temperature of 450 °C is reached (point 3). This temperature value might seem high, but the phenomena are so fast that we can assume that PEI and PEEK do not have time to be entirely degraded by such temperatures. Then, the polymer flows until reaching a maximal flow corresponding to a travel of around 250 μm (point 4). As the theoretical PEI thickness was 750 μm at the test beginning, it is assumed that only PEI has flowed and PEEK has not started to melt. Finally, a fast cooling at around 600 K s^{-1} occurs in stage 5. As PEI is an amorphous polymer, the cooling does not impact its physical structure. Besides, the cooling rate does not impact PEEK either, as it was assumed that PEEK had not reached its melting temperature during welding. These temperature and travel curves are chosen as reference for the following section, and they are used in the next figures for comparison with other welding parameters (Figs. 8 and 9). Further analysis of these typical steps are presented in the following section.

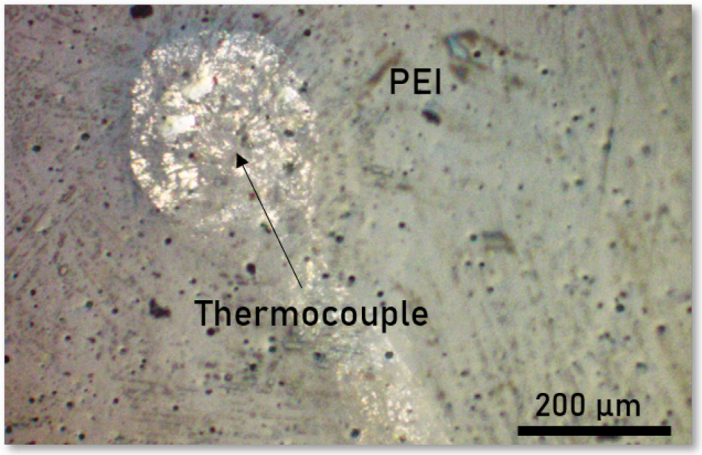

Fig. 5. Micrograph of an embedded thermocouple within the PEI layer.

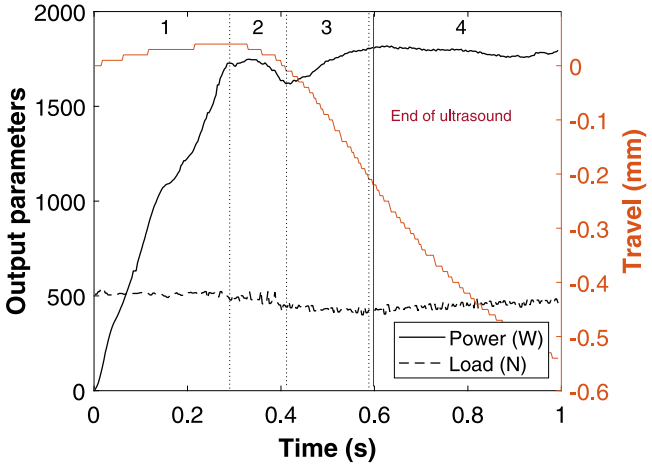

Fig. 6. Typical power, load and displacement curves during ultrasonic welding of CF/PEEK + PEI specimens for a amplitude of 32 µm, a welding load of 500 N and a welding time of 1000 ms.

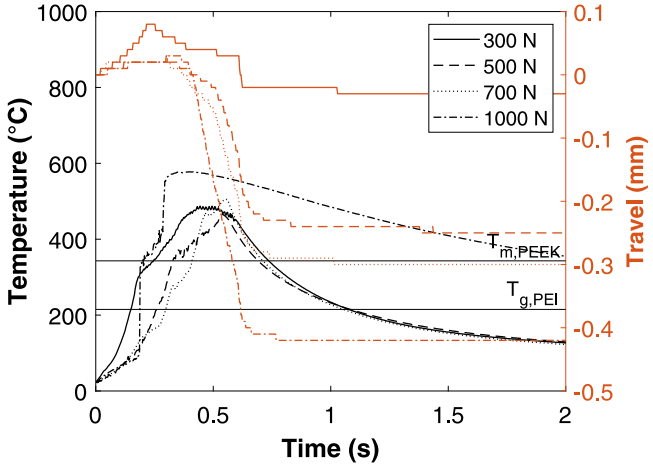

Fig. 8. Temperature profiles and sonotrode travel during USW for a amplitude of 32 µm and a welding time of 600 ms for a 0.75 mm-thickness energy director.

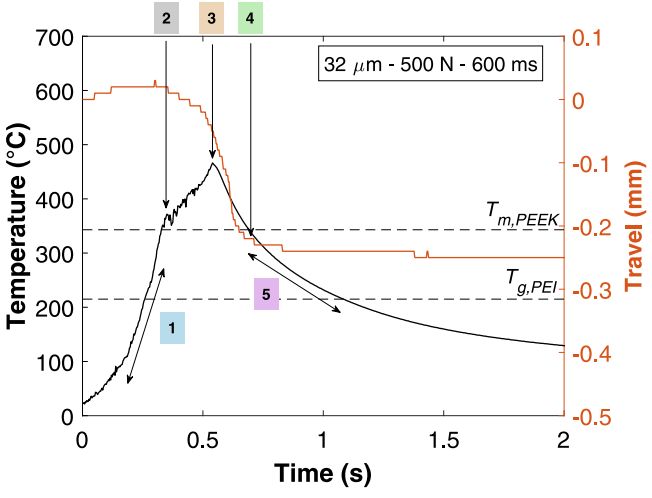

Fig. 7. Temperature and travel curves for the following welding conditions: amplitude of 32 µm, 500 N welding load and 600 ms welding time showing different steps (1 to 5).

3.3. Welding parameter influence on heat profiles

To evaluate the welding parameters influence on temperature profiles, several measurements were completed by increasing only one parameter at a same time. Figs. 8 and 9 show the combined (temperature and travel) data to evaluate the influence of, respectively, welding time, amplitude and welding load.

Fig. 8 presents the sonotrode travel and temperature measurements for five different welding loads. First of all, temperature curves do not show a similar behavior. For instance, the 500 N curve exhibits a sharp peak whereas the 300 N curve is rounded at its top. This difference may be attributed to the localization of hot-spots nucleation that can be more or less close from the thermocouple during heating stage. The heating stage is not linear for each welding load. They all display a change of slope that can be associated with the beginning of a physical change in the polymer structure, namely the beginning of softening or melting. The melting temperature T_m(PEEK) and glass transition temperature T_g(PEI) are symbolized by horizontal lines in Fig. 8. According to this curves, this change seems to occur right after reaching PEEK melting temperature. However, heating rates are fast (around 1000 K s^{-1}). As it has been shown in the literature, the heating rate shifts towards higher melting temperature. Upon fast heating, the polymer reaches a metastable state called superheating. As demonstrated by Minakov et al. [28] on linear PET, isotactic polypropylene (iPP) and isotactic polystyrene (iPS), the superheating magnitude $\Delta T = T_m - T_0$ with

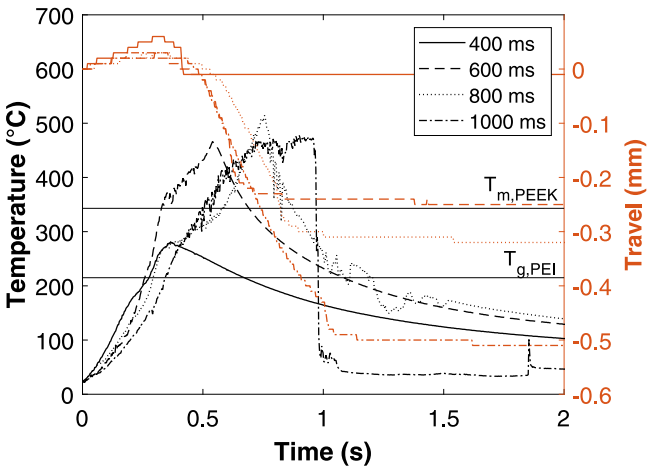

Fig. 9. Influence of welding time on temperature profiles and sonotrode travel during USW (amplitude: 32 μm, welding load: 500 N, energy director thickness: 0.75 mm).

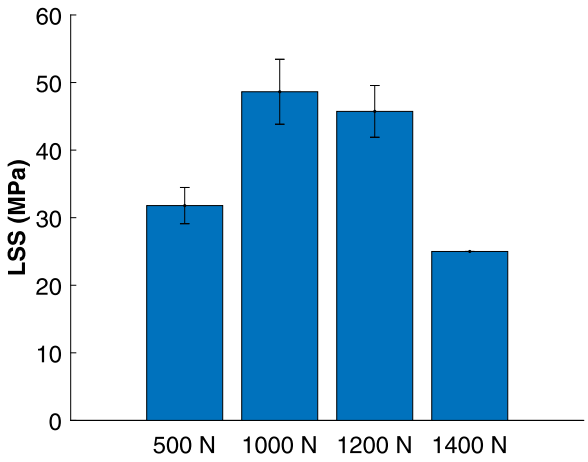

Fig. 10. Lap shear strength for different values of welding load (amplitude: 32 μm and, welding time: 600 ms and 0.75 mm-thickness energy director).

T_m the measured melting temperature and T_0 the melting temperature at equilibrium, depends on the melting process kinetics and increases with the heating rate. For instance, ΔT = 30 K with a heating ramp of 1000 K s^{-1} for PET. Besides, the glass transition temperature of PEI is equal to 217 °C measured by Differential Scanning Calorimetry (DSC). To this end, considering the fast heating, the beginning of temperature slope during heating stage – right after the melting temperature of PEEK – could be associated with PEI glass transition. Moreover, the travel curves start decreasing at the same location where a change in the temperature slope occurs. An hypothesis is that softening of the energy director affects the temperature profiles. The hypothesis is worth being validated by ultra fast DSC for future works. We assume that the melting temperature shift revealed by Minakov et al. would be similar to a glass transition shift for amorphous polymer. When load increases from 300 N to 700 N, the temperature reaches a maximum temperature close to 500 °C for a few hundreds of milliseconds before decreasing. This peak is associated with the end of the ultrasonic vibration.

The cooling behavior appears to be similar for all these testing conditions and is around 600 K s^{-1}. PEI is an amorphous polymer, which means that the cooling rate do not affect much its mechanical properties, in comparison with semi-crystalline ones for which a high cooling ramp inhibits the crystallization. The crystallinity affects the mechanical properties as revealed by Martineau [29]. E' is at 2.9 GPa for amorphous PEEK whereas it reaches 3.5 GPa for crystallized PEEK. The elongation rate is also affected.

As it can be seen in Fig. 8, travel curves are quite different when mechanical load rises from 300 N to 700 N. The 300 N curve shows that the polymer has started to heat but did not reach a full softened/melted state since its final displacement is around zero. The welding load was not high enough to create an intimate contact that could ensure an efficient friction and homogeneous heat generation at the interface, despite the value of temperature measured. The 500 N and 700 N welding load curves reach respectively 0.25 mm and 0.3 mm negative displacement of the sonotrode, meaning that PEI film has started to squeeze, losing 0.25 mm and 0.3 mm of its initial thickness. On the other hand, the 1000 N test exhibits a different behavior with a maximal temperature close to 580 °C, and where temperature stays above 400 °C for a much longer time. In parallel, travel reaches a final level of 0.4 mm, much higher than for the other welding conditions. In all welding load testing conditions, the final thickness of the interface does not seem to have lost more than 0.3 mm from its initial thickness, which would confirm that the CF/PEEK plies have not been submitted to squeeze flow and therefore have not been enough thermally affected to reach the melting temperature of PEEK.

Similar experiments were made when varying the vibration amplitude. The results are presented as supplementary information. It appears that the amplitude does not have a strong impact on the temperature measurement since the curves look similar.

Other factors may affect welding, such as surface roughness or local heat nucleation points that may change the temperature profile and could be predominant in those results. Also, PEI film has an initial thickness of 0.25 mm with a standard deviation of 0.04 mm. This variation is significative when comparing with the difference of 0.1 mm in the final travel values.

Finally, Fig. 9 shows the temperature profiles and travel for different welding time values. As seen in Fig. 8, a change of heating ramp is noticed on those curves, related to softening of PEI, except for the 400 ms curve where maximum measured temperature is below 300 °C. For this time, it can also be seen that the final travel is close to zero, confirming that PEI did not soften even if the T_g of PEI at equilibrium is close to 220 °C. Heating rates seem to be similar for all welding times as for the various welding loads investigated (Fig. 8). This shows a good repeatability of the welding test. The uncertainty of measurement on the temperature is evaluated at ± 30 °C while the error on the displacement is around ± 0.02 mm. From 600 ms to 1000 ms, the curves reach a peak close to 500 °C. However, the 1000 ms curve seems to reach a temperature plateau for a few hundred of milliseconds before temperature drop at the end of ultrasound loading. This could favor the motion of macromolecular chains which have more time to diffuse and entangle before the temperature goes down. It can also be seen that the final travel increases with the increase of welding time, from 0.25 mm to 0.5 mm for respectively 600 ms and 1000 ms, confirming a larger squeeze flow for higher loading times. Finally, the curve at 1000 ms must have been affected by another phenomenon since the temperature curve drops from 450 °C to 25 °C in no time. From 1 s, it can be assumed that the curve is not exploitable. An explanation could be the break of the thermocouple due to friction. The small peak at 1.8 s in the temperature curve support this hypothesis.

3.4. Influence of the welding parameters on the mechanical properties

Single lap shear tests are carried out in order to evaluate the mechanical properties of the welds, and the results are shown in Figs. 10 and 11. Fig. 10 shows the LSS results for the different values of welding load investigated. The LSS tends to increase up to a maximal value of 49 MPa at 1000 N. After that, the LSS starts decreasing. Before 1000 N, it can be assumed that the intimate contact between the two specimens is not sufficient. The fracture surface of welded specimens in similar welding conditions is presented in Section 3.4. As a consequence, the

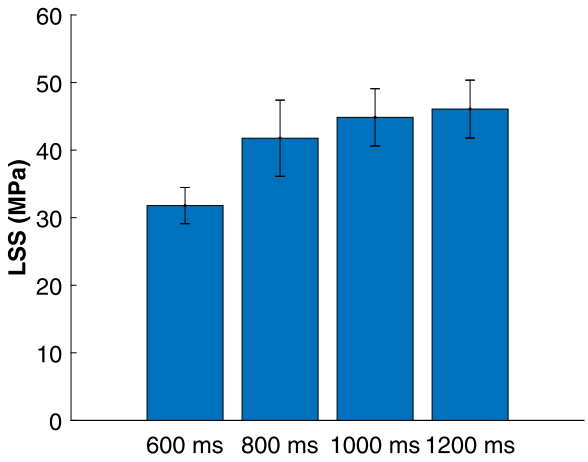

Fig. 11. Lap shear strength for different values of welding time (amplitude: 32 µm, welding load: 500 N and 0.75 mm-thickness energy director).

friction of the specimens is too low to induce local heating over the total contact area. Even if the temperature would reach the flowing temperature of the polymers, the contact area is too low to allow the macromolecular chain of PEI to diffuse and entangle at the interface.

The fracture surfaces of the welded specimens after lap shear tests have been observed by optical microscopy to understand the crack propagation within the interphase. The interfacial fracture surface at 500 N reveals two different fracture mechanisms in Fig. 12(a). For all fractures, only one side of each specimen is presented. Firstly a failure occurs within the PEI layer as shown by the absence of fiber in the right of the picture. The other mode is a failure within the CF/PEEK layers, as fibers are observed on the left of the same picture. A deeper analysis of the fracture modes is presented in Section 3.5. At 1000 N and 1200 N, respectively Fig. 12 (b_1) and (b_2), a failure within PEI also takes place on a smaller surface than 500 N, explaining why the mechanical properties are lower. Indeed, a failure within the composite is better because it shows that the PEI bond at the interface is stronger than the adhesion between CF/PEEK layers within the specimens. However, when increasing the welding load above 1000 N, the LSS decreases but the one at 1200 N remains higher than the one at 500 N as CF/PEEK failure is prevailing at 1200 N. Unmelted areas of PEI are also observed in Fig. 12 (b_3) at 1400 N, which would suggest that the vibration was not sufficient to melt the energy director homogeneously. It is also worth noting that at 1500 N, the specimens are not welded at all, meaning that the welding load was too high to allow any sonotrode vibration to occur. From this, we can conclude that welding over 1200 N hinders the sonotrode vibration. This phenomenon shows a limitation in the use of ultrasonic welding for which the highest loads lead to no vibration at all.

Lap shear strength for different values of amplitude is presented as a supplementary information. As for temperature measurements, the mechanical strength does not seem to be impacted by a change in the amplitude

The LSS values for several welding times are plotted in Fig. 11. LSS values tend to increase when increasing the welding time. Welding times under 1000 ms, Fig. 12(a) and (d_1), present cohesive failures within the PEI layer for almost half of the welded surface, explaining their lower LSS. This confirms the hypothesis made in Fig. 8 that 1000 ms is a suitable welding condition. At 1000 ms, LSS values are slightly lower than the maximum found when investigating the influence of the welding load (i.e. 49 MPa). This could be explained by the interfacial surface of the weld. The fracture surfaces look similar, i.e. with a majority occurring with the PEI interface. However, the fracture at 1000 ms seems to have a little bit more PEI fracture on the right side, as seen in Fig. 12 (d_2). At 1200 ms, a maximum LSS of 46 MPa is achieved but still slightly lower than 49 MPa. A possible explanation is that PEEK and carbon fibers have started to flow on one side (black arrow on the picture in Fig. 12 (d_3)). Another hypothesis might be that lap shear test is not an optimal option to evaluate the mechanical strength of welded joints as some mechanisms (i.e. flow of PEEK and carbon fibers) are not quantified with this technique. To conclude this section, the welding time has a strong influence on the mechanical properties as it increases the LSS. The limitation is

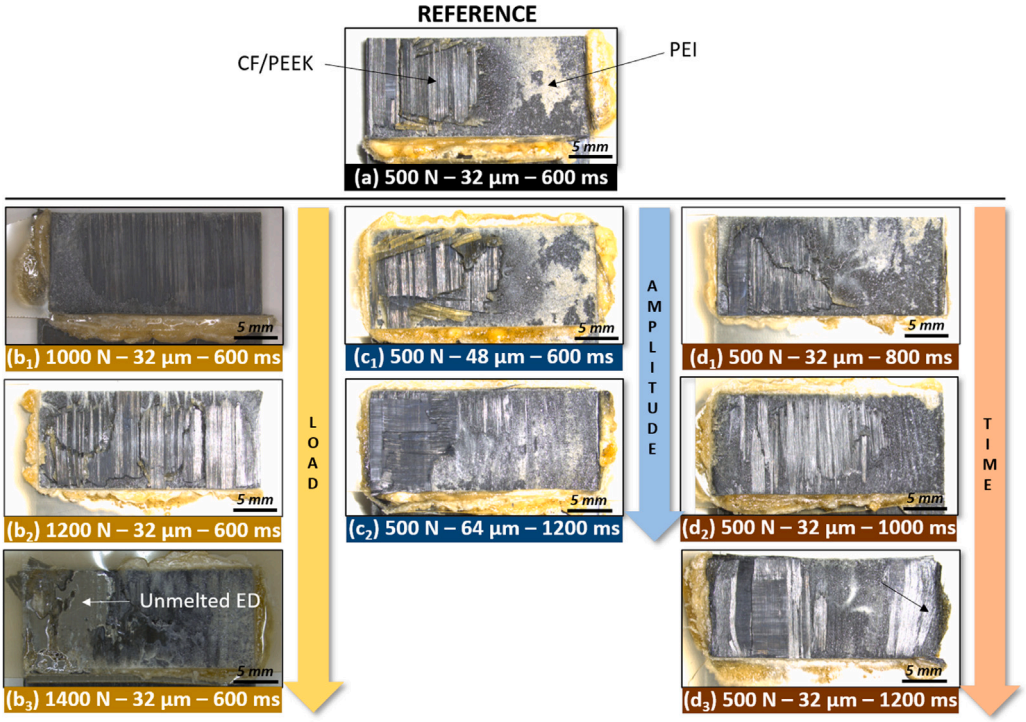

Fig. 12. Interfacial fracture of welded specimens in several welding conditions.

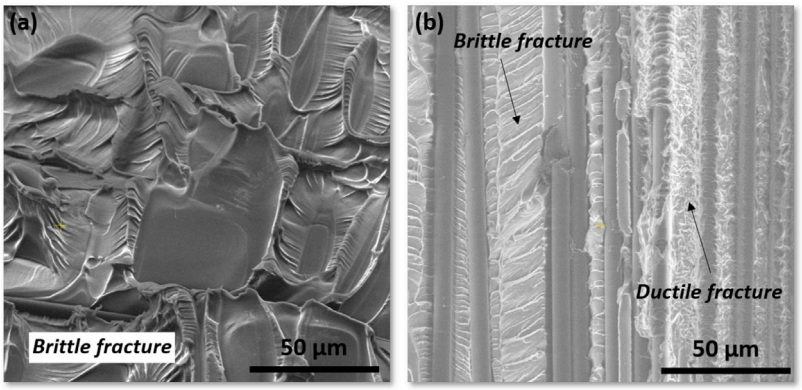

Fig. 13. SEM micrographs of PEI-localized fracture (a) and PEEK-localized fracture (b).

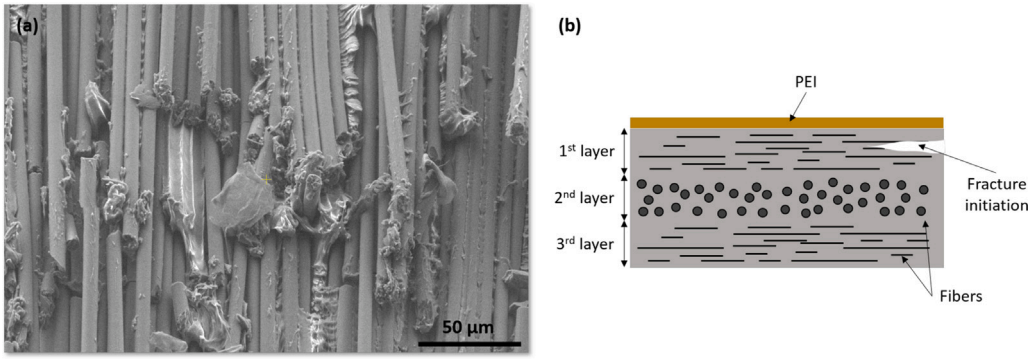

Fig. 14. Cohesive failure within the CF/PEEK layer.

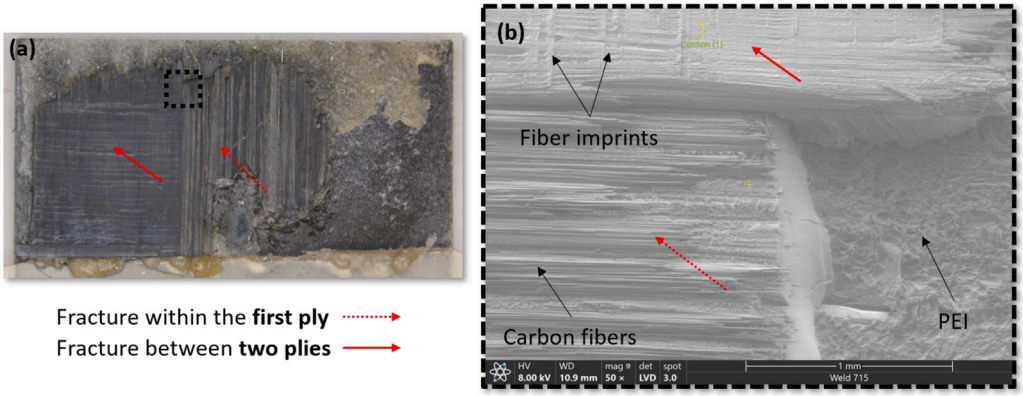

Fig. 15. Interfacial cohesive failure APC-2 plies through SEM and optical micrographs.

when PEEK and carbon fibers start flowing at the edges, decreasing mechanical strength linked to the alignment of the fibers. Thus, it can be assumed that a longer time (i.e. above 1200 ms) would not imply an increase of LSS since the polymer matrix and carbon fibers would likely squeeze and flow even more, and LSS would drop.

For all welding loads except 1400 N, the values of LSS seem competitive with what can be found in the literature. Tsiangou et al. [30] reached 43 MPa using similar materials (CF/PEEK and 0.25-mm-thick PEI energy director). Villegas et al. [15] found LSS values at 39 MPa for CF/PEI specimens with a PEI energy director and 35 MPa for CF/PPS specimens with a PPS energy director [24]. Tao et al. [20] worked on US welding of CF/PEEK associated with a PEEK energy director and measured a LSS at 28 MPa. Regarding other bonding processes, it was found by Li et al. [31] a 46 MPa value of LSS for CF/PEEK resistance welded joints and a 49 MPa value by Smiley et al. [32] using Thermabond™ process on CF/PEEK specimens with a PEI interlayer. Those results show that ultrasonic welding of CF/PEEK using a PEI energy director compete with industrially advanced bonding processes.

LSS is the most widely used mechanical test to characterize the interfacial resistance of welded assemblies: it is easy to implement and does not require any specimen preparation. Even if LSS is suitable for comparing welding conditions, it does not give information on the crack propagation resistance, unlike cleavage and double cantilever beam (DCB) tests for measuring the initiation and propagation values of Mode I fracture energy G_I. Moreover, the comparison of LSS values of US welding to other welding processes is not deeply evident since the whole thermomechanical history undergone during the process impacts the mesostructure of the welded specimens. Depending on the process, either the entire thickness or only the interface area is melted. Therefore, the final morphology or crystallinity of the materials can

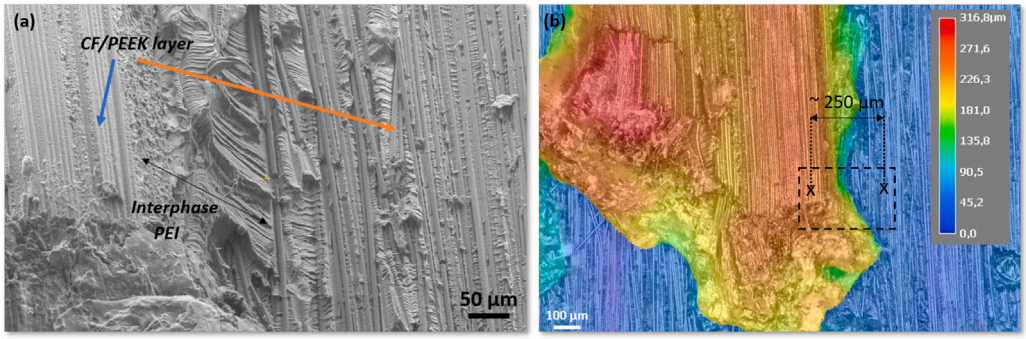

Fig. 16. SEM micrograph of interfacial fracture between two layers of CF/PEEK (a) and optical micrograph of the same location (b).

vary from one process to another due to the impact of the cooling rate. Moreover, an assembling process involving a squeeze flow at the interface makes difficult the reproducibility of the fracture initiation.

3.5. Microscopic study on interfacial fracture mechanisms

Different fracture mechanisms were highlighted in Section 3.4, i.e. a rupture within the PEI interface and a rupture within the CF/PEEK layers. The hereby section aims to go deeper in analyzing the fracture mechanisms. Fig. 13 shows SEM images of PEI-localized fracture (13(a)) and PEEK-localized fracture (13(b)). PEI-localized fracture seems to be associated with brittle-type fracture whereas PEEK-localized fracture is a combination of brittle and ductile fractures. When considering brittle fracture in PEEK, cracks appear to initiate on one side at the fiber/matrix interface and to propagate transversely until they reach another fiber. In other zones, a rugged surface stems from the stretching of the polymer matrix, this is representative of a ductile fracture.

Moreover, another type of fracture is observed in our specimens: fiber breakage. Fig. 14(a) displays fracture within a CF/PEEK layer where fiber fracture is predominant. Most of the fiber surfaces are smooth, indicating a poor fiber/matrix adhesion. It suggests that fracture within the composite specimen is cohesive, i.e. within a CF/PEEK layer as seen in Fig. 14(b). In this scenario, the crack initiates close to the PEI-rich zone and propagate inside the first CF/PEEK ply. Fig. 15 shows the interfacial fracture of a weld that exhibits both cohesive and adhesive failure within APC-2 plies. Fig. 15(a) is an optical micrograph from the entire welding area after the lap shear test. Fig. 15(b) is the SEM micrograph of the black square in Fig. 15(a). The full red arrows point out a fracture between two APC-2 plies (the first and second plies). Indeed, fiber imprints in the perpendicular direction of the first layer can be seen, meaning that the fracture happened between two plies. The red dotted arrows show fibers from the first ply. In that case, the fibers have been pulled out, confirming that a cohesive fracture within one ply occurs.

For the welding conditions leading to LSS above 30 MPa, the welded surface is very rugged. An example is presented in Fig. 16. In this SEM image (Fig. 16(a)), two layers of PEEK/CF are visible, separated by a PEI-rich interphase. It is obvious that the visible layers of CF/PEEK are not from the same composite specimen from the height difference of 250 µm measured by optical microscopy (Fig. 16(b)). The layer on the left belongs to the lower specimen whereas the layer on the right belongs to the upper specimen, in Fig. 16. An hypothesis is that cracks initiate in both welded PEEK/CF specimens. When propagating from one specimen to another, the cracks go through the PEI-rich interphase, giving rise to this rough surface. In the interfacial zone, PEEK and PEI are blended due to their miscibility. The concentration gradient of PEI comes from the preparation of welding specimens. During manufacturing, the cycle time is long enough to promote the interdiffusion of PEI and PEEK macromolecular chains. The next section aims to go further in analyzing the composition of such interphase. The thickness of this gradient and its influence on the mechanical properties and fracture mechanisms are not fully understood yet and need further investigation.

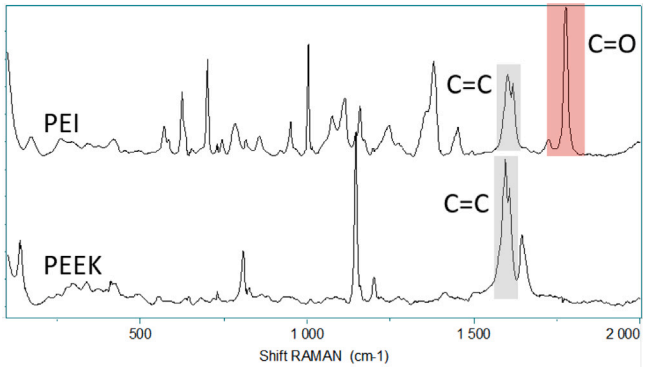

Fig. 17. Raman spectrum of PEEK, PEI and carbon fibers.

3.6. Composition of PEI/PEEK interphase in the welded zone

Miscibility of PEEK and PEI is attested in the literature [33]. The characteristic time of PEEK have been measured by DMA and it is around 2 s at 350 °C [14], while it is a few ms for PEI at 270 °C [34]. From this data, diffusion of PEI inside PEEK matrix is expected. Raman spectroscopy was used to quantify the PEI concentration along the interphase. The spectra given in Fig. 17 shows one distinct band at 1777 cm^{-1} (red area) [35,36] attributable to the νC=O bond of PEI. In addition, the area between 1550–1620 cm^{-1}, attributable to $\nu C{=}C_{cycle}$ (amorphous or crystalline phase) of PEI and PEEK (gray area in Figs. 17 and 18) is selected.

Fig. 19(b) and (c) show mapping of the same interfacial zone after welding. The mapping area goes from the first ply of APC-2 from specimen 1 to the first ply of APC-2 from specimen 2, going through the entire PEI layer, as seen in Fig. 19(a). Fig. 19(b) is done from the ratio of the band relative intensities of C=O (PEI) and C=C (PEEK + PEI). In the map, the edges of the first plies of APC-2 exhibit black color, which correspond to 100% PEEK. When getting closer to the center, green color appears under -100 µm and above 100 µm, meaning that the ratio PEI/(PEI + PEEK) is higher than at the edges. It corresponds to a blend of PEI/PEEK in the first plies of both specimens. This blend comes from the diffusion of PEI during specimen manufacturing. The thickness of the blend is around 25 µm. At the center of the map (from -100 µm to 75 µm), the highest ratio is obtained, around 1. As expected, pure PEI is predominant in that zone.

Fig. 19(c) uses a two components multicurve regression with the complete spectra of PEI and PEEK. Overall, the same observation can be made compared to the previous map. Indeed, the 100% PEEK zone

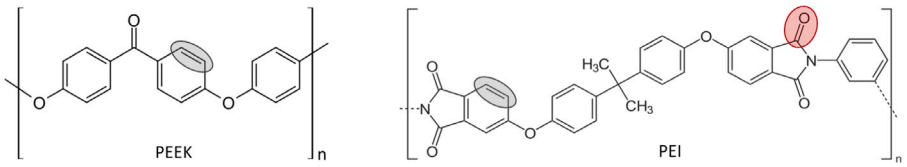

Fig. 18. Chemical bonds (red and gray) analyzed on Raman spectroscopy for PEEK and PEI.

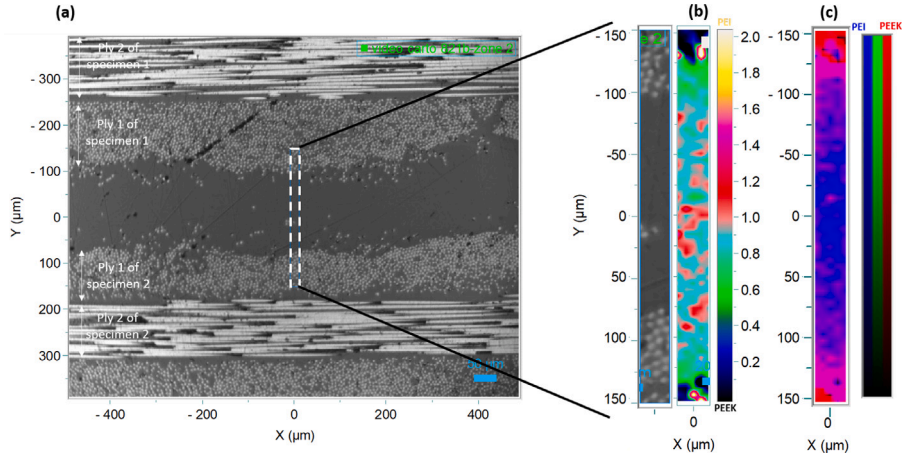

Fig. 19. Optical micrograph of the welding interface (a) and mapping of interfacial zone using the ratio of the band relative intensities of PEI and PEEK (b) and using a multicurve regression (c).

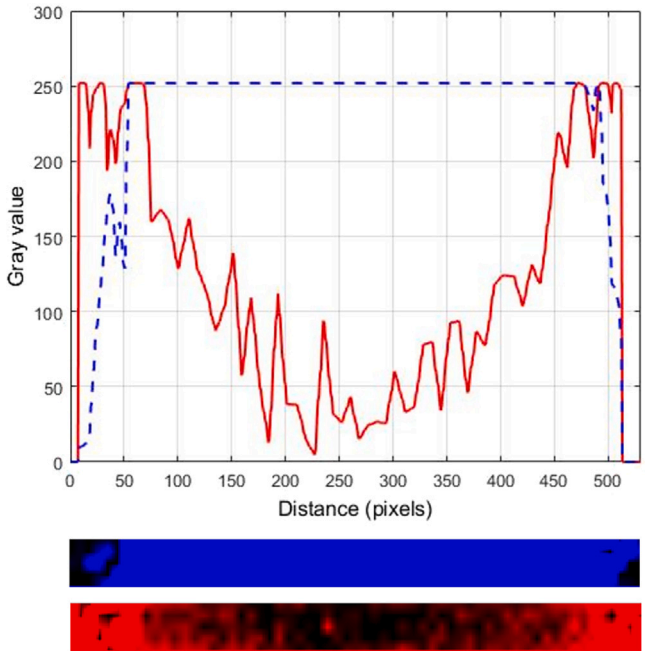

Fig. 20. Intensity profile from Fig. 19(c), PEI in blue and PEEK in red. 500 pixels = 300 um.

can be observed in red and the blend is visible in pink (mixed color: blue + red = pink). In that case, the thickness of the blend seems to be higher than in the previous map because the treatments used are not the same and they do not have the same measurement accuracy. A whole pink zone is visible with a length of around 25 µm on each side, corresponding to the first plies of APC-2. However, large zones of around 50 µm on each side (between -100 µm and -50 µm and between 50 µm and 100 µm) present a blue and pink color mix. It probably means that the PEI/PEEK blend is present in that area to a lesser extent than in the first plies. Finally, a large area between -50 µm and 50 µm is mainly PEI due to the strong blue color. It can be imagined that increasing or decreasing this 100-µm-length PEI-based area would not affect the mechanical strength of welds. In addition, a pink dot is visible in that area. It is associated with a fiber that has moved through the ED. The fibers take along some part of the matrix when moving. Due to the dot pink color, it is assumed that a PEI/PEEK blend surrounds fibers. The technique used in Fig. 19(c) looks more precise than Fig. 19(b), as the fibers can be detected.

The original image in Fig. 19(c) is an RGB color image. The red channel corresponds to PEEK, and the blue one to PEI. We use the "split channels" function in ImageJ to have two different images, one corresponding to PEEK and the other one to PEI. Then, for each image, using the "plot profile" function in ImageJ, the intensity profile, averaged over the whole width of the image has been plotted in Fig. 20. Both profiles look symmetrical on both sides of the assembly. The PEI concentration is constant in the center and a concentration gradient is observed on the 50 pixels on each side, meaning 30 µm. We retain this width of 30 µm as the interdiffusion thickness. However, the PEEK concentration slowly decreases from each side to the center, indicating a possible contribution of carbon fiber signal on Raman spectroscopy response.

4. Conclusion

This study contributes to a better understanding of the effect of process parameters on mechanical strength of CF/PEEK composites assembled by ultrasonic welding. This work involves a PEI interlayer for assembling CF/PEEK composites as a way to prevent deconsolidation and degradation due to overheating. This study rationalizes the influence of welding parameters (welding load, amplitude and welding time) on the temperature profiles and the mechanical properties of welded joints. As the interface is a closed contact during welding, measuring the temperature at the interface is tricky. For the first time, we provide thermal profiles from microthermocouples located close to the interface. Then, the mechanical strength of the assemblies have

been characterized by LSS tests. The work focus on three parameters, namely welding load, welding time and the vibration amplitude.

We demonstrate that the welding load has a strong influence on thermal history and mechanical resistance and fracture modes. The maximal temperature was achieved at 1000 N and was close to 580 °C but for a short time, ensuring the diffusion of the PEI chains while avoiding the degradation of the PEEK matrix. In this welding condition, the maximum LSS was found at 49 MPa which is high compared to values in the literature when referring to CF/PEEK assembling, whatever the process. Welding load can increase the LSS value of the welded specimens until reaching a threshold limited by the ability of the welder to vibrate accordingly to the operator's request. When the welding load exceeds 1200 N, the welder cannot vibrate to its full capacity.

Finally, in the same way as welding load, welding time is the time during which the ultrasounds are applied. The LSS of the resulting joints increases with the welding time. In this case, however, a longer welding time can lead to a squeeze flow and sometimes degradation of the polymer at the welded interface. Besides, the maximum LSS was found at 47 MPa (welding time of 1000 ms), and the maximum temperature is 100 °C lower than the one found with the optimum welding load of 1000 N.

In summary, two optimum welding conditions were found (500 N–1000 ms–32 μm & 1000 N–600 ms–32 μm), exhibiting similar fracture surfaces but different temperature profiles. This means that, when dealing with ultrasonic welding of thermoplastics, several optimum welding parameter settings lead to similar mechanical strengths and interfacial fractures.

Interfacial fracture mechanisms have been analyzed by microscopy and Raman mapping. A PEEK-based fracture leads to the highest mechanical strengths whereas PEI-based fracture is noticed for lower LSS. High strength welds exhibit fracture from one specimen to the other one, going through the entire thickness of PEI-rich interphase. A gradient of concentration is present at the interface with a thickness of around 0.075 mm, due to interdiffusion of PEI and PEEK during specimen manufacturing.

CRediT authorship contribution statement

Margot Bonmatin: Conceptualization, Methodology, Investigation, Visualization, Data curation, Writing – original draft. **France Chabert:** Conceptualization, Methodology, Validation, Writing – review & editing, Supervision, Funding acquisition. **Gérard Bernhart:** Conceptualization, Methodology, Validation, Writing – review & editing, Supervision, Funding acquisition, Project administration. **Thierry Cutard:** Methodology, Validation, Writing – review & editing. **Toufik Djilali:** Conceptualization, Methodology, Validation, Supervision, Resources.

Declaration of competing interest

The authors declare the following financial interests/personal relationships which may be considered as potential competing interests: INP-ENIT-University of Toulouse reports financial support was provided by LAUAK Group.

Data availability

Data will be made available on request.

Acknowledgments

This work was funded by LAUAK Group. The authors are grateful to Olivier Marsan, INP-ENSIACET, University of Toulouse, France, for performing Raman spectroscopy.

Appendix A. Supplementary data

Supplementary material related to this article can be found online at https://doi.org/10.1016/j.compositesa.2022.107074.

References

[1] Yousefpour A, Hojjati M, Immarigeon J-P. Fusion bonding/welding of thermoplastic composites. J Thermoplast Compos Mater 2004;17(4):303–41.
[2] Fernandez Villegas I, Moser L, Yousefpour A, Mitschang P, Bersee HE. Process and performance evaluation of ultrasonic, induction and resistance welding of advanced thermoplastic composites. J Thermoplast Compos Mater 2013;26(8):1007–24.
[3] Wise RJ. Thermal welding of polymers. Woodhead Publishing; 1999.
[4] Voyutskii SS, Vakula VL. The role of diffusion phenomena in polymer-to-polymer adhesion. J Appl Polym Sci 1963;7(2):475–91. http://dx.doi.org/10.1002/app.1963.070070207, URL https://onlinelibrary.wiley.com/doi/abs/10.1002/app.1963.070070207, _eprint: https://onlinelibrary.wiley.com/doi/pdf/10.1002/app.1963.070070207.
[5] Vasenin RM. Adhesion pressure in the diffusion theory of the adhesion of polymers. Polym Sci U.S.S.R. 1962;3(4):608–15. http://dx.doi.org/10.1016/0032-3950(62)90322-2, URL https://www.sciencedirect.com/science/article/pii/0032395062903222.
[6] De Gennes P-G. Reptation of a polymer chain in the presence of fixed obstacles. J Chem Phys 1971;55(2):572–9. http://dx.doi.org/10.1063/1.1675789, URL https://aip.scitation.org/doi/abs/10.1063/1.1675789.
[7] De Gennes P-G. Comptes rendus de l'académie des sciences. C R Acad Sci B 1980;291:219–21.
[8] Brochard-Wyart F. Kinetics of polymer—Polymer interdiffusion. In: Lee L-H, editor. Fundamentals of adhesion. Boston, MA: Springer US; 1991, p. 181–206. http://dx.doi.org/10.1007/978-1-4899-2073-7_6.
[9] Wool RP, Yuan B-L, McGarel OJ. Welding of polymer interfaces. Polym Eng Sci 1989;29(19):1340–67. http://dx.doi.org/10.1002/pen.760291906, URL https://onlinelibrary.wiley.com/doi/abs/10.1002/pen.760291906.
[10] Lee WI, Springer GS. A model of the manufacturing process of thermoplastic matrix composites. J Compos Mater 1987;21(11):1017–55. http://dx.doi.org/10.1177/002199838702101103, Publisher: SAGE Publications Ltd STM.
[11] Mantell SC, Springer GS. Manufacturing process models for thermoplastic composites. J Compos Mater 1992;26(16):2348–77. http://dx.doi.org/10.1177/002199839202601602, Publisher: SAGE Publications Ltd STM.
[12] Yang F, Pitchumani R. A fractal cantor set based description of interlaminar contact evolution during thermoplastic composites processing. J Mater Sci 2001;36(19):4661–71. http://dx.doi.org/10.1023/A:1017950215945.
[13] Levy A, Heider D, Tierney J, Gillespie JW. Inter-layer thermal contact resistance evolution with the degree of intimate contact in the processing of thermoplastic composite laminates. J Compos Mater 2014;48(4):491–503.
[14] Bonmatin M, Chabert F, Bernhart G, Djilali T. Rheological and crystallization behaviors of low processing temperature poly(aryl ether ketone). J Appl Polym Sci 2021;138(47):51402.
[15] Fernandez Villegas I. Strength development versus process data in ultrasonic welding of thermoplastic composites with flat energy directors and its application to the definition of optimum processing parameters. Composites A 2014;65:27–37.
[16] Palardy G, Fernandez Villegas I. Ultrasonic welding of thermoplastic composites with flat energy directors: Influence of the thickness of the energy director on the welding process. In: ICCM 20: 20th international conference on composite materials, Copenhagen, Denmark, 19-24 July 2015. 2015.
[17] Fernandez Villegas I. In situ monitoring of ultrasonic welding of thermoplastic composites through power and displacement data. J Thermoplast Compos Mater 2015;28(1):66–85.
[18] Fernandez Villegas I, Grande BV, Bersee HEN, Benedictus R. A comparative evaluation between flat and traditional energy directors for ultrasonic welding of CF/PPS thermoplastic composites. Compos Interfaces 2015;22(8):717–29.
[19] Senders FJM. Continuous ultrasonic welding of thermoplastic composites (Master of Science Thesis), Delft University of Technology; 2016.
[20] Tao W, Su X, Wang H, Zhang Z, Li H, Chen J. Influence mechanism of welding time and energy director to the thermoplastic composite joints by ultrasonic welding. J Manuf Process 2019;37:196–202.
[21] Benatar A, Gutowski TG. Ultrasonic welding of PEEK graphite APC-2 composites. Polym Eng Sci 1989;29(23):1705–21.
[22] Liu S-J, Chang I-T, Hung S-W. Factors affecting the joint strength of ultrasonically welded polypropylene composites. Polym Compos 2001;22(1):132–41.
[23] Fernandez Villegas I, Bersee HE. Ultrasonic welding of advanced thermoplastic composites: An investigation on energy-directing surfaces. Adv Polym Technol 2010;29(2):112–21.
[24] Fernandez Villegas I, Palardy G. Ultrasonic welding of CF/PPS composites with integrated triangular energy directors: melting, flow and weld strength development. Compos Interfaces 2017;24(5).

[25] Palardy G, Fernandez Villegas I. On the effect of flat energy directors thickness on heat generation during ultrasonic welding of thermoplastic composites. Compos Interfaces 2017;24(2).
[26] Levy A, Le Corre S, Fernandez Villegas I. Modeling of the heating phenomena in ultrasonic welding of thermoplastic composites with flat energy directors. J Mater Process Technol 2014;214(7):1361–71.
[27] Thévenet J. Développement d'une métrologie thermique des contacts glissants en freinage (Ph.D. thesis), Valenciennes; 2009, URL https://theses.fr/2009VALE0016.
[28] Minakov AA, Wurm A, Schick C. Superheating in linear polymers studied by ultrafast nanocalorimetry. Eur Phys J E 2007;23(1):43.
[29] Martineau L, Chabert F, Bernhart G, Djilali T. Mechanical behavior of amorphous PEEK in the rubbery state. In: ECCM17 — 17th European conference on composite materials. Munich, Germany; 2016.
[30] Tsiangou E, Teixeira de Freitas S, Fernandez Villegas I, Benedictus R. Ultrasonic welding of epoxy- to polyetheretherketone- based composites: Investigation on the material of the energy director and the thickness of the coupling layer. J Compos Mater 2020;54(22):3081–98.
[31] Li X, Zhang T, Li S, Liu H, Zhao Y, Wang K. The effect of cooling rate on resistance-welded CF/PEEK joints. J. Materials Research and Technology 2021;12:53–62.
[32] Smiley AJ, Chao M, Gillespie JW. Influence and control of bondline thickness in fusion bonded joints of thermoplastic composites. In: Flow Processes in Composite Materials '91, Composites Manufacturing In: Flow Processes in Composite Materials '91, 1991;2(3).223–32,
[33] Crevecoeur G, Groeninckx G. Binary blends of poly(ether ether ketone) and poly(ether imide): miscibility, crystallization behavior and semicrystalline morphology. Macromolecules 1991;24(5):1190–5. http://dx.doi.org/10.1021/ma00005a034.
[34] Mudarra M, Belana J, Cañadas JC, Diego JA, Sellarès J, Dıaz-Calleja R, Sanchıs MJ. Space charge relaxation in polyetherimides by the electric modulus formalism. J Appl Phys 2000;88(8):4807–12. http://dx.doi.org/10.1063/1.1312839, URL https://aip.scitation.org/doi/abs/10.1063/1.1312839. Publisher: American Institute of Physics.
[35] Samyn P, Schoukens G. Tribochemical reactions on polyimide sliding surfaces evaluated with Raman spectroscopy and atomic force microscopy. Surf Interface Anal 2008;40(3–4):853–7.
[36] Devasahayam S, Hill DJT, Connell JW. FT-Raman studies of a range of polyimides subjected to high-energy radiations at room and elevated temperatures. J Appl Polym Sci 2006;101(3):1575–82.